Nanoscale

PAPER

View Article Online
View Journal | View Issue

Cite this: *Nanoscale*, 2023, **15**, 2837

Efficient and bright green InP quantum dot light-emitting diodes enabled by a self-assembled dipole interface monolayer†

Lufa Li,‡[a] Yaning Luo,‡[a] Qianqian Wu,[a] Lin Wang,[a] Guohua Jia,[b] Tao Chen,[c] Chengxi Zhang *[a] and Xuyong Yang *[a]

Received 26th November 2022,
Accepted 5th January 2023

DOI: 10.1039/d2nr06618a

rsc.li/nanoscale

The interfacial state between the hole transport layer (HTL) and quantum dots (QDs) plays a crucial role in the optoelectronic performance of light-emitting diodes. Herein, we reported an efficient and bright green indium phosphide (InP) QD-based light-emitting diode (LED) by introducing a self-assembled monolayer of 4-bromo-2-fluorothiophenol (SAM-BFTP) molecule to improve interfacial charge transport in LED devices. The molecular dipole layer at the interface of the QD layer and HTL not only reduces the energy barrier of holes injected into QDs through vacuum energy level shift but also inhibits the fluorescence quenching of QDs caused by the HTL. Moreover, copper ions doped into phosphomolybdic acid (Cu:PMA) is selected as the hole injection layer (HIL) into the device system based on the SAM-BFTP molecule, and as a result, a green InP QD LED (QLED) with a maximum external quantum efficiency (EQE) of 8.46% and a luminance of 18 356 cd m^{-2} was realized. This work can inform and underpin the future development of InP-based QLEDs with concurrent high efficiency and brightness.

1. Introduction

Colloidal quantum dots (QDs) are considered to be the next generation emitting materials for light-emitting diodes (LEDs) on account of their tunable fluorescence spectrum, wide color gamut, high color purity and excellent optoelectronic properties.[1–5] Among the numerous cadmium-free QD materials, indium phosphide (InP) is regarded as a strong competitor due to its comparable optical properties to cadmium-based QDs.[6–11] Despite the fast progress in the development of InP-based QD LEDs (QLEDs), the green InP QLEDs still suffer from poor device performance compared with the recently reported red InP QLEDs with an external quantum efficiency (EQE) of over 20%.[12] This has slowed the practical application of InP QLEDs in full-color displays and other optoelectronics.

ZnMgO can serve as an efficient electron transport layer (ETL) for QLEDs due to its matched energy levels with QDs and high electron mobility.[13–18] However, the high electron mobility of ZnMgO and the small barrier difference between ZnMgO ETL and InP QDs as compared to that of between poly (9,9-dioctylfluorene-*co*-*N*-(4-butyl phenyl) diphenylamine) (TFB) hole transport layer (HTL) and InP QDs result in the disequilibrium of carrier injection. The accumulation of excess electrons at the interface of QDs and HTL will act as non-radiative recombination centers that deteriorate device efficiency, device lifetime and increase turn-on voltage.[19–22] Numerous strategies have been utilized to solve the problem of electron surplus to balance charge injection; for example, *N*,*N*′-bis(3-methyl phenyl)-*N*,*N*′-bis(phenyl)-9,9-dioctylfluorene (DOFL-TPD) organic molecules mixed with red InP/ZnSe/ZnS QDs to form a homogeneous film due to the excellent compatibility of long alkyl chains of DOFL-TPD and oleic acid ligands on the QD surface, hole injection and energy transfer are facilitated, making the charge carrier recombination more balanced and efficient.[23] Short alkyl thiols were introduced into CdSe/ZnS QDs to induce bandgap changes of QDs, causing valence band edge shift and thus reducing the hole injection barrier.[24] Reducing the charge transfer capability of the ETL is also a common way to improve the charge balance of the device. By using poly(*p*-phenylene benzobisoxazole) (TBS-PBO) as an electron-blocking layer (EBL), excess electron injection into the QDs can be blocked, resulting in a better charge carrier

[a]*Key Laboratory of Advanced Display and System Applications of Ministry of Education, Shanghai University, 149 Yanchang Road, Shanghai 200072, China. E-mail: Andrew_xiwa@shu.edu.cn, yangxy@shu.edu.cn*
[b]*School of Molecular and Life Sciences, Curtin University, Perth, WA 6102, Australia*
[c]*Office of Admissions and Career Services, Shanghai University, 99 Shangda Road, Shanghai 200444, China*

†Electronic supplementary information (ESI) available. See DOI: https://doi.org/10.1039/d2nr06618a

‡These authors contributed equally to this work.

balance.[25,26] Vacuum energy level translation or interfacial dipole moment are generated by introducing interfacial layers such as polymethyl methacrylate (PMMA) and polyethyleneimine ethoxylation (PEIE), thus reducing the energy level potential barrier to improving the brightness and efficiency of the device.[1,27,28] Moreover, the hygroscopic/acidic nature of organic poly(3,4-ethylenedioxythiophene):polystyrene sulfonate (PEDOT:PSS) will negatively affect the device stability.[29,30] Although some progress has been made by balancing charges to improve device efficiency, the modification of the interfacial state between the HTL and QD emission layer (EML) to enhance the hole injection and to suppress the effect on the fluorescence quenching of the QD EML still needs to be further explored.

In this study, we report a simple and effective interface layer regulation method to increase the hole injection of the device and reduce electron leakage toward trap sites in TFB HTL, thus enabling high-performance QLEDs. In particular, two-dimensional dipolar organic self-assembled monolayer 4-bromo-2-fluorothiophenol (SAM-BFTP) with docking group, backbone and the functional head group is grafted onto the surface of TFB, which not only adjusts the electronic energy level to balance charge injection into QDs but also passivates the trap states on the surface. With the further use of an inorganic hole injection layer (HIL) of copper ions doped phosphomolybdic acid (Cu:PMA), the SAM-BFTP-based QLED shows significant improvement in device performance (peak brightness = 18 356 cd m^{-2}, peak EQE = 8.46%, a half-lifetime is prolonged 3.8 h at an initial brightness of 1500 cd m^{-2}).

2. Results and discussion

2.1. Charge injection for the PEDOT:PSS/TFB-based device

In this study, green-emitting InP/ZnSe/ZnS QDs with a photoluminescence quantum yield (PLQY) of ~82% and grain size of 7.5–8.0 nm are used as the emitter to fabricate the QLED (Fig. S1†) and the PEDOT:PSS-based QLED was used as the control device, as shown in Fig. 1a. The energy level values for indium tin oxide (ITO), PEDOT:PSS and ZnMgO are taken from previously published reports,[31,32] and the energy level values of InP/ZnSe/ZnS QDs and TFB are measured through ultraviolet photoelectron spectroscopy (UPS) and optical absorption spectroscopy (Fig. S2†). The as-prepared QLED exhibited an EL peak of 535 nm and the full-width-at-half-peak (FWHM) of 43 nm, which redshifted by ~2 nm compared to the PL peak of the InP QD solution due to the interdot interactions between tightly packed QDs in the solid film and the Stark effect caused by the electric field (Fig. 1b).[3] The control device showed a maximum luminance of 1792 cd m^{-2}, a turn-on voltage of 2.5 V and a maximum EQE of 3.7%. However, the notable current density fluctuation within 0–2 V indicates the presence of a certain amount of leakage current in the device, which is known to be an important factor affecting the durability of the device.[33] In addition, the electron injection barrier (0.3 eV) between ZnMgO ETL and InP QDs is significantly

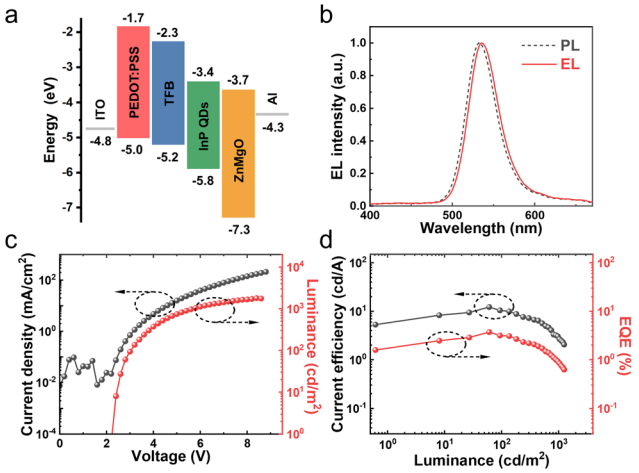

Fig. 1 (a) Energy level diagram for PEDOT:PSS-based QLED. (b) Normalized PL and EL spectra of QDs and PEDOT:PSS-based QLED. (c) *J*–*L*–*V* and (d) CE–EQE–*L* characteristics for PEDOT:PSS-based QLED.

smaller than that of between TFB HTL and InP QDs (0.6 eV) (Fig. 1a), which makes it easier for electrons to be injected into the InP QD EML, resulting in the charge carrier injection imbalance of QLED devices. Such an unbalanced carrier injection will reduce device efficiency, operational lifetime and increase turn-on voltage.[34]

2.2. Effect of the BFTP interface layer on the electrical properties of the InP QD layer

To coordinate the injection rate of electrons and holes into the QDs in the working device, we modify the energy level of the TFB HTL by introducing BFTP as an interfacial molecular dipole layer (<3 nm) to reduce the hole injection barrier between the TFB HTL and the QD EML. BFTP acts as a two-dimensional SAM (Fig. S3†) with a docking group (thiophenol group), backbone benzene ring and functional head group (bromine group and fluorine group at different positions of the benzene ring).[35] The BFTP molecules are densely arranged on the surface of the TFB by the coordination of the thiophenol group, and the functional head group is attached to the QDs. The charge interaction between the functional head group and the thiophenol group induces an electric field to generate an interfacial dipole moment (Fig. 2a).[36,37]

To verify the effect of interfacial layer BFTP on the fluorescence properties of the InP QD layer, we performed fluorescent lifetime and PLQY of InP QD films deposited on the TFB and TFB/BFTP layer, respectively. The BFTP-modified film exhibits enhanced PL intensity and a longer lifetime compared with the untreated film. The PL intensity of the BFTP-modified film enhances 1.5-fold (Fig. S5†) when the BFTP proportion is 5 vol%, corresponding to the PLQY of the InP QD film increases from 31% to 48%, and the PL lifetime rising from 28.9 to 49.2 ns (Fig. 2c, d and Table 1). This means that the introduction of the interfacial layer BFTP effectively passivates the surface defect states of the organic HTL, thereby reducing the influence of the organic HTL on the fluorescence quench-

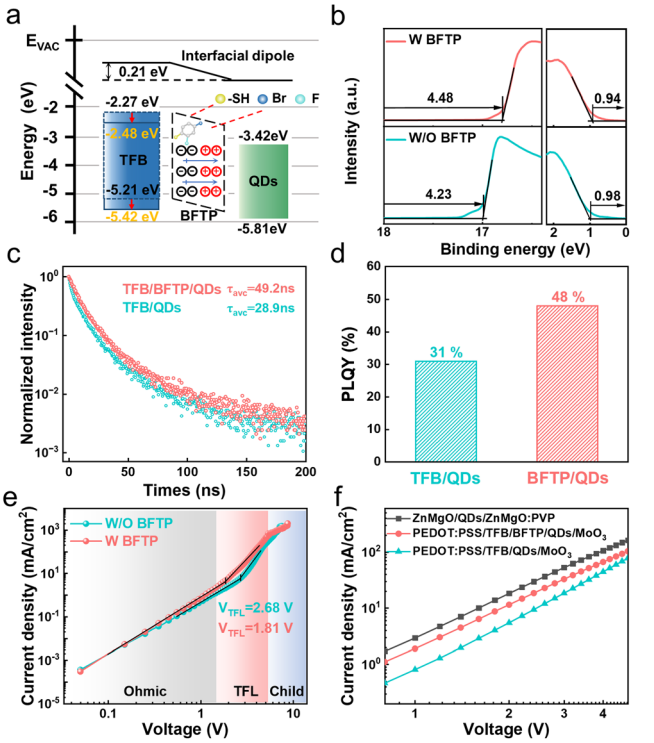

Fig. 2 (a) Schematic mechanism diagram of BFTP regulatory TFB energy level and BFTP molecular formula. (b) UPS spectra of with BFTP and without BFTP films deposited on ITO/PEDOT:PSS/TFB substrates. (c) Time-resolved PL of QDs on TFB and TFB/BFTP films. (d) PLQYs of QDs in TFB and TFB/BFTP films. Current–voltage characteristics of devices constructed with (e) ITO/TFB/QDs/MoO_3/Al and ITO/TFB/BFTP/QDs/MoO_3/Al configuration utilized for estimating the defect density in QD films. (f) *J*–*V* characteristics of electron-only and hole-only device based on different HTLs.

Table 1 Fluorescence lifetimes and PLQYs of QDs upon different films. Data in the table are derived from fits to the measured TRPL curves with two exponential-decay functions. Here τ_i is the lifetime of one decay component and A_i is fractional amplitude; τ_{ave} is an average lifetime given by = $(A_1\tau_1^2 + A_2\tau_2^2 + A_3\tau_3^2)/(A_1\tau_1 + A_2\tau_2 + A_3\tau_3)$

Sample	A_1	τ_1 (ns)	A_2	τ_2 (ns)	A_3	τ_3 (ns)	τ_{ave} (ns)	PLQY (%)
TFB/QDs	0.07	1.67	0.61	10.2	0.32	38.5	28.9	31
TFB/BFTP/QDs	0.49	19.1	0.37	7.4	0.14	82.9	49.2	48

ing of the EML, which is beneficial for high-performance QLEDs.

UPS analysis combined with the optical absorption spectra was conducted to evaluate the molecular dipole layer BFTP on the effect of valence band maxima (E_{VBM}) of the TFB film. UPS result shows that the E_{VBM} of the TFB film has decreased from −5.21 eV to −5.42 eV (Fig. 2b), indicating that the interfacial energy barrier has reduced by 0.21 eV. The BFTP molecular modification causes a bending potential distribution of HTL near the QDs, which result in a decreased energy barrier between HTL and EML. A more matched energy level is beneficial to the injection of holes. Moreover, the balanced charge carrier injection can reduce the accumulation of electrons at the interface of QDs and HTL, thereby suppressing the emission quenching of InP QDs.[38]

The defect states of the TFB HTL after BFTP interface modification were verified by implementing the space charge limited current (SCLC) characterization. The current–voltage (*I*–*V*) characteristics were measured from hole-only devices with the structure of ITO/TFB/QDs/MoO_3/Al and ITO/TFB/BFTP/QDs/MoO_3/Al. The *I*–*V* characteristic curve can be divided into three parts: the Ohmic region, the trap-filled-limit (TFL) region, and the Child region.[39] At a low voltage (ohmic region), the interface is ideal for an ohmic contact interface, allowing sufficient charge to be injected from the electrode into the InP QDs. The *I*–*V* curve begins to transition into the TFL region at the onset voltage (V_{TFL}), where the current increases rapidly indicating that all defect states are filled. Therefore, defect state density is reflected by V_{TFL} and is proportional to V_{TFL} (Fig. S4†). The V_{TFL} is about 2.68 V before the interface modification (Fig. 2e). However, the V_{TFL} drops to 1.81 V after TFB HTL modified by the BFTP molecular dipole layer, corresponding to the defect density decreases from 3.19×10^{17} to 1.48×10^{16} (Fig. S4†), which reflects the defects of the TFB HTL are significantly reduced after the interface modification. This is consistent with enhanced PL intensity. The lower defect density for TFB/BFTP is beneficial for the suppression of electron trapping at the interface between the HTL and QDs, boosting the radiative recombination efficiency in the InP QD EML.

2.3. Effect of the BFTP interface layer on the film morphology of the InP QD layer

The effect of hydrophilicity of TFB layer modified by interfacial layer BFTP was also investigated. The contact angle for the TFB/BFTP film decreases from 23.1° to 8.9° compared with the TFB film (Fig. 3a), indicating that the surface hydrophilicity of the TFB/BFTP film is increased. The thiophenol group in BFTP can improve the wetting ability of the InP QD solution, which is more conducive to the formation of the dense and uniform high-quality InP QD film. Furthermore, the surface roughness (r.m.s) of the InP QD film also decreases from 2.72 to 1.54 nm (Fig. 3c). In addition, the similar transmittance of the TFB/BFTP thin film compared with the TFB film indicates the introduction of the interface layer does not degrade the luminescence performance of device in the test procedure (Fig. S7†).

2.4. QLED devices based on the BFTP interface layer and Cu: PMA HIL

To confirm the enhanced hole injection capability of TFB/BFTP, we fabricated the hole-only device with the structure of ITO/PEDOT:PSS/(TFB/BFTP or TFB)/QDs/MoO_3/Al and electron-only device with the structure of ITO/ZnMgO/QDs/ZnMgO:PVP/Al for comparison (Fig. 2f). By introducing the BFTP interface layer, the hole density is increased by an order of magnitude compared with the control device, which is closer to the electron-only device, indicating a significant

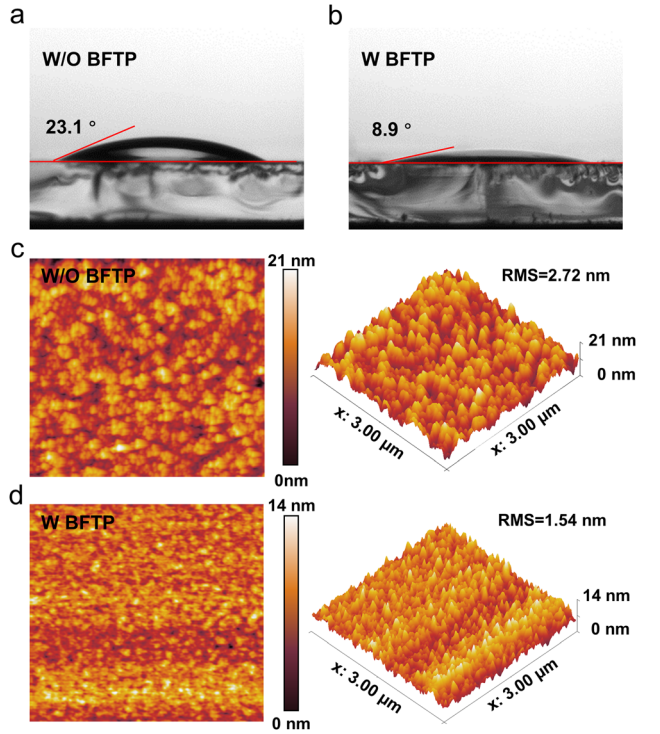

Fig. 3 Images of water contact angles of (a) TFB and (b) TFB/BFTP films. Atomic force microscopy (AFM) images of QDs deposited onto (c) TFB and (d) TFB/BFTP film surface.

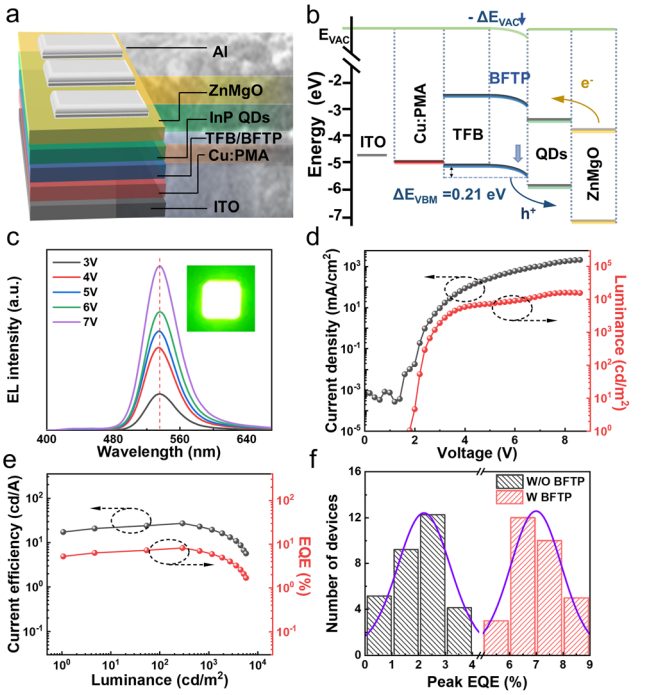

Fig. 4 (a) Device structure with the cross-sectional TEM image. (b) Band variation diagram employing BFTP on TFB HTL. The interface dipoles induce vacuum level shifts (Δ_{VAC}) to modify the potential profile across the device. (c) EL spectrum of BFTP-based QLEDs with different voltages. (d) *J*–*L*–*V* and (e) CE–EQE–*L* characteristics for BFTP-based QLEDs. (f) Peak EQEs of QLEDs based on TFB/BFTP (W BFTP) and TFB (W/O BFTP) HTL tested from 30 devices.

enhancement of the hole injection capability. PMA, an inorganic metal–oxide material, has been used as HIL to improve device efficiency and stability due to its high carrier mobility and chemical/thermal stability.[40] To further increase the hole injection in QLEDs, the Cu:PMA (the electrical properties of the PMA were adjusted by copper ion doping) is selected as HIL due to the lower hole injection barrier (0.3 eV) compared with PEDOT:PSS (0.4 eV). A more matched energy level favours the carrier injection equilibrium and enhances the performance of the device. The *J*–*V* characteristics of the hole-only device and the electron-only device also demonstrated that Cu:PMA as HIL helps to improve the performance of devices (Fig. S8 and S9†). At the same time, we verified the transmittance and device performance of Cu:PMA (Fig. S10 and S11†).

Encouraged by the above findings, green-emitting InP QLED with the structure of ITO/Cu:PMA/TFB/BFTP/QDs/ZnMgO/Al was fabricated (Fig. 4a). The flat-band energy diagram of QLED after BFTP modification is shown in Fig. 4b. The TFB/BFTP-based QLEDs show a stable EL peak under different driving voltages, a turn-on voltage of 1.8 V, a maximum brightness of 18 356 cd m^{-2} and an average EQE of 7.1% (Fig. 4c and d). The EQE value presented here is an average measured for 30 devices and the maximum EQE of TFB/BFTP-based QLEDs is up to 8.45% (Fig. 4e and f), which is ~2.3 times higher than that of PEDOT:PSS/TFB-based LEDs (EQE ~3.7%). The leakage current of 0–2 V drops by an order of magnitude (Fig. 4d) compared to the control device (Fig. 1c), demonstrating that the defects at the interface are significantly reduced, and the carrier injection is more balanced and effective by adjusting the energy level, thus enabling high brightness and efficiency of the QLED device. We added the important parameters of the QLEDs under different control conditions in Table S1.†

The operational stability of QLEDs is a crucial condition for their practical application. We investigated the lifespan of TFB/BFTP-based all-solution QLEDs with different HIL (PEDOT:PSS, PMA and Cu:PMA). The Cu:PMA/TFB/BFTP-based QLED exhibits a greatly improved half-lifetime with T_{50} = 3.82 h at an initial luminance of 1500 cd m^{-2} (acceleration factor n = 1.8, Fig. S12†), which is 6.3 times (100 cd m^{-2}, 500 h) longer than that of PEDOT:PSS/TFB-based QLED (T_{50} = 80 h@100 cd m^{-2}) (Fig. S12†). This is mainly attributed to the Cu:PMA having better thermal stability than the organic PEDOT:PSS, and meanwhile, the hygroscopic/acidic nature of organic PEDOT:PSS corrodes the ITO electrodes, causing a negative effect on device operational stability.[41]

3. Conclusions

In summary, we fabricated an efficient, bright, and stable InP-based QLED by employing the SAM-BFTP layer to modify the

underlying HTL, which is found to be of great importance to balance charge carrier injection due to the increased hole injection caused by the generated interfacial dipole moment. Moreover, the interface layer effectively inhibits the fluorescence quenching of the InP QD EML due to the improved interfacial contact where the defects are passivated. In addition, with the further use of copper dopant in inorganic PMA HIL, the all-solution-processed green InP QLED with a high performance of turn-on voltage of 1.8 V, peak EQE of ~8.5% and peak luminance over 18 000 cd m^{-2} is achieved, and a greatly improved half-lifetime with T_{50} = 3.82 h@1500 cd m^{-2}, which is 6.3 times (100 cd m^{-2}, 500 h) longer than that of PEDOT:PSS/TFB-based QLED (T_{50} = 80 h@100 cd m^{-2}).

4. Experimental section

4.1. Materials and synthesis

Anhydrous ethanol (99.5%), anhydrous methanol (99.5%), and ethyl acetate (>99.5%) were purchased from Acros. PEDOT:PSS and TFB were acquired from Aladdin. Phospho-molybdic acid hydrate (99%), chlorobenzene (99.9%) and BFTP were purchased from Alfa-Aesar. Zinc acetate dihydrate (>99%), magnesium acetate tetrahydrate (>98%), copper acetate hydrate (>99%), tetramethylammonium hydroxide (>97%), and dimethyl sulfoxide (>99.9%) were purchased from Sigma-Aldrich. All chemicals were used without further purification.

The precursor solution of PMA was prepared by dissolving phosphomolybdic acid hydrate in anhydrous ethanol (13 mg ml^{-1}). Copper acetate hydrate (10 mg) was introduced in the PMA precursor solution to form a Cu:PMA precursor solution. BFTP was dissolved in an anhydrous ethanol solution with 5 vol% and stirred for 1 h. For the ZnMgO solution, zinc acetate dihydrate and magnesium acetate tetrahydrate (molar ratio:10 : 1) were dissolved in dimethyl sulfoxide (DMSO) solution to a precursor with a concentration of 0.1 M, then the 10 mL of 0.5 M tetramethylammonium hydroxide (TMAH) ethanol solution was added gradually to the above precursor solution and stirred for 2 h to form ZnMgO nanoparticles. The mixture was then washed with ethyl acetate three times and dispersed in ethanol at a concentration of 30 mg ml^{-1} for the device's fabrication.

4.2. Fabrication of LEDs

ITO substrates with a resistance of 15 Ω per square were cleaned by ultrasonication in deionized water, acetone and isopropyl alcohol for 15 min each. The dry ITO substrates were treated with oxygen plasma for 15 min to improve the hydrophilicity and work function. The HIL PEDOT:PSS or Cu:PMA was spin-coated onto the ITO substrates at 4000 rpm for 40 s and annealed at 150 °C for 15 min in air atmosphere. The TFB (8 mg ml^{-1}, chlorobenzene) was spin-coated at 3000 rpm for 40 s and baked at 120 °C for 20 min. Subsequently, the BFTP solution was spin-coated at 2500 rpm for 40 s, followed by annealing at 80 °C for 5 min. The QDs and ZnMgO were spin-coated at 3000 rpm, 2000 rpm for 40 s, then annealed at 60 °C for 10 min and 90 °C for 20 min, respectively. After depositing of the ZnMgO film, TPBI (40 nm) and LiF/Al electrode (1 nm/100 nm) were sequentially deposited by thermal evaporation at a base pressure of around 4×10^{-4} Pa.

4.3. Characterization methods

XPS and UPS measurements were performed by using a Thermo Fischer ESCALAB 250Xi. The surface morphology of the perovskite films was characterized by atomic force microscopy (AFM, Seiko instrument SPA 400). The absorption spectra and transmittance were conducted using a PerkinElmer Lambda 950 UV-vis-NIR spectrometer. Cross-sectional field emission scanning electron microscopy (FE-SEM) was conducted by a JEOL JSM-7500F microscope. The morphology of InP QDs was analyzed by transmittance electron microscopy (TEM, JEM-2100F, Cold Field Emission Type, JEOL). The PL lifetime was measured by using an Edinburgh FLS920 spectrometer. The half-lifetime of QLEDs was tested through a ZJZCL-1 OLED ageing lifespan test instrument. The performance of QLEDs was investigated by a Shenzhen Pynect integrated sphere (50 cm in diameter) system equipped with Keithley 2400 sourcemete and QEPro spectrograph. The device structures used by SCLC were ITO/TFB/QDs/MoO_3/Al and ITO/TFB/BFTP/QDs/MoO_3/Al. The structure of the electron-only device was ITO/ZnMgO/QDs/ZnMgO:PVP/Al. The structure of hole-only was ITO/PEDOT:PSS/TFB/QDs/MoO_3/Al and ITO/PEDOT:PSS/TFB/BFTP/QDs/MoO_3/Al.

Conflicts of interest

There are no conflicts to declare.

Acknowledgements

The authors would like to thank the financial support from the National Key Research and Development Program of China (2022YFE0200200), National Natural Science Foundation of China (62174104, 61735004 and 52102182) and the Program of Shanghai Academic/Technology Research Leader (22XD1421200), China Postdoctoral Science Foundation (2020M680054, 2021T140440).

References

1 D. Kim, Y. Fu, S. Kim, W. Lee, K.-H. Lee, H. K. Chung, H.-J. Lee, H. Yang and H. Chae, *ACS Nano*, 2017, **11**, 1982–1990.
2 H. Moon, C. Lee, W. Lee, J. Kim and H. Chae, *Adv. Mater.*, 2019, **31**, 1804294.
3 B. S. Mashford, M. Stevenson, Z. Popovic, C. Hamilton, Z. Zhou, C. Breen, J. Steckel, V. Bulovic, M. Bawendi, S. Coe-Sullivan and P. T. Kazlas, *Nat. Photonics*, 2013, **7**, 407–412.

4 O. Wang, L. Wang, Z. Li, Q. Xu, Q. Lin, H. Wang, Z. Du, H. Shen and L. S. Li, *Nanoscale*, 2018, **10**, 5650–5657.
5 Q. Wu, X. Gong, D. Zhao, Y.-B. Zhao, F. Cao, H. Wang, S. Wang, J. Zhang, R. Quintero-Bermudez, E. H. Sargent and X. Yang, *Adv. Mater.*, 2022, **34**, 2108150.
6 P. Ramasamy, N. Kim, Y.-S. Kang, O. Ramirez and J.-S. Lee, *Chem. Mater.*, 2017, **29**, 6893–6899.
7 D. Hahm, J. H. Chang, B. G. Jeong, P. Park, J. Kim, S. Lee, J. Choi, W. D. Kim, S. Rhee, J. Lim, D. C. Lee, C. Lee, K. Char and W. K. Bae, *Chem. Mater.*, 2019, **31**, 3476–3484.
8 E.-P. Jang, J.-H. Jo, S.-W. Lim, H.-B. Lim, H.-J. Kim, C.-Y. Han and H. Yang, *J. Mater. Chem. C*, 2018, **6**, 11749–11756.
9 W. Shen, H. Tang, X. Yang, Z. Cao, T. Cheng, X. Wang, Z. Tan, J. You and Z. Deng, *J. Mater. Chem. C*, 2017, **5**, 8243–8249.
10 J. Lim, M. Park, W. K. Bae, D. Lee, S. Lee, C. Lee and K. Char, *ACS Nano*, 2013, **7**, 9019–9026.
11 Q. Wu, F. Cao, S. Wang, Y. Wang, Z. Sun, J. Feng, Y. Liu, L. Wang, Q. Cao, Y. Li, B. Wei, W.-Y. Wong and X. Yang, *Adv. Sci.*, 2022, **9**, 2200959.
12 Y.-H. Won, O. Cho, T. Kim, D.-Y. Chung, T. Kim, H. Chung, H. Jang, J. Lee, D. Kim and E. Jang, *Nature*, 2019, **575**, 634–638.
13 H. Moon, W. Lee, J. Kim, D. Lee, S. Cha, S. Shin and H. Chae, *Chem. Commun.*, 2019, **55**, 13299–13302.
14 Y.-L. Shi, F. Liang, Y. Hu, M.-P. Zhuo, X.-D. Wang and L.-S. Liao, *Nanoscale*, 2017, **9**, 14792–14797.
15 Z. Zhong, J. Zou, C. Jiang, L. Lan, C. Song, Z. He, L. Mu, L. Wang, J. Wang, J. Peng and Y. Cao, *Org. Electron.*, 2018, **58**, 245–249.
16 L. Wang, J. Lin, X. Liu, S. Cao, Y. Wang, J. Zhao and B. Zou, *J. Phys. Chem. C*, 2020, **124**, 8758–8765.
17 S. Guo, Q. Wu, L. Wang, F. Cao, Y. Dou, Y. Wang, Z. Sun, C. Zhang and X. Yang, *IEEE Electron Device Lett.*, 2021, **42**, 1806–1809.
18 J. Jing, L. Lin, K. Yang, H. Hu, T. Guo and F. Li, *Org. Electron.*, 2022, **103**, 106466.
19 Y. Yang, Y. Zheng, W. Cao, A. Titov, J. Hyvonen, J. R. Manders, J. Xue, P. H. Holloway and L. Qian, *Nat. Photonics*, 2015, **9**, 259–266.
20 F. So and D. Kondakov, *Adv. Mater.*, 2010, **22**, 3762–3777.
21 S. Chen, X. Jiang and F. So, *Org. Electron.*, 2013, **14**, 2518–2522.
22 C. Coburn and S. R. Forrest, *Phys. Rev. Appl.*, 2017, **7**, 041002.
23 M. G. Han, Y. Lee, H.-I. Kwon, H. Lee, T. Kim, Y.-H. Won and E. Jang, *ACS Energy Lett.*, 2021, 1577–1585.
24 L. Wang, Y. Lv, J. Lin, J. Zhao, X. Liu, R. Zeng, X. Wang and B. Zou, *J. Mater. Chem. C*, 2021, **9**, 2483–2490.
25 D. Li, J. Bai, T. Zhang, C. Chang, X. Jin, Z. Huang, \B. Xu and Q. Li, *Chem. Commun.*, 2019, **55**, 3501–3504.
26 X. Jin, C. Chang, W. Zhao, S. Huang, X. Gu, Q. Zhang, F. Li, Y. Zhang and Q. Li, *ACS Appl. Mater. Interfaces*, 2018, **10**, 15803–15811.
27 S. Rhee, D. Hahm, H.-J. Seok, J. H. Chang, D. Jung, M. Park, E. Hwang, D. C. Lee, Y.-S. Park, H.-K. Kim and W. K. Bae, *ACS Nano*, 2021, **15**, 20332–20340.
28 X. Dai, Z. Zhang, Y. Jin, Y. Niu, H. Cao, X. Liang, L. Chen, J. Wang and X. Peng, *Nature*, 2014, **515**, 96–99.
29 H. Shen, W. Cao, N. T. Shewmon, C. Yang, L. S. Li and J. Xue, *Nano Lett.*, 2015, **15**, 1211–1216.
30 D. I. Son, B. W. Kwon, D. H. Park, W.-S. Seo, Y. Yi, B. Angadi, C.-L. Lee and W. K. Choi, *Nat. Nanotechnol.*, 2012, **7**, 465–471.
31 J.-H. Jo, J.-H. Kim, K.-H. Lee, C.-Y. Han, E.-P. Jang, Y. R. Do and H. Yang, *Opt. Lett.*, 2016, **41**, 3984–3987.
32 Q. Su, H. Zhang and S. Chen, *Appl. Phys. Lett.*, 2020, **117**, 053502.
33 F. Tian, Y. Zhu, Z. Xu, B. Li, X. Zheng, Z. Ni, H. Hu, Y. Chen, J. Zhuang, L. Wu, D. Fu, X. Yan and F. Li, *IEEE Electron Device Lett.*, 2020, **41**, 1384–1387.
34 F. Cao, Q. Wu and X. Yang, *ACS Appl. Mater. Interfaces*, 2019, **11**, 40267–40273.
35 K.-G. Lim, S. Ahn and T.-W. Lee, *J. Phys. Chem. C*, 2018, **6**, 2915–2924.
36 L. Qian, Y. Zheng, J. Xue and P. H. Holloway, *Nat. Photonics*, 2011, **5**, 543–548.
37 G. Heimel, F. Rissner and E. Zojer, *Adv. Mater.*, 2010, **22**, 2494–2513.
38 F. Cao, Q. Wu, Y. Sui, S. Wang, Y. Dou, W. Hua, L. Kong, L. Wang, J. Zhang, T. Jiang and X. Yang, *Small*, 2021, **17**, 2100030.
39 M. You, H. Wang, F. Cao, C. Zhang, T. Zhang, L. Kong, L. Wang, D. Zhao, J. Zhang and X. Yang, *ACS Appl. Mater. Interfaces*, 2020, **12**, 43018–43023.
40 D. Dong, L. Lian, H. Wang and G. He, *Org. Electron.*, 2018, **62**, 320–326.
41 F. Cao, H. Wang, P. Shen, X. Li, Y. Zheng, Y. Shang, J. Zhang, Z. Ning and X. Yang, *Adv. Funct. Mater.*, 2017, **27**, 1704278.

